CHIN. PHYS. LETT. Vol. 33, No. 10 (2016) 108201

Analysis of Dissociation Mechanism of CO_2 in a Micro-Hollow Cathode Discharge *

Jiang-Ling Cheng(程将领), Hai-Xing Wang(王海兴)**, Su-Rong Sun(孙素蓉)

School of Astronautics, Beijing University of Aeronautics and Astronautics, Beijing 100191

(Received 11 June 2016)

Considering the feature of distributions of parameters within the micro-hollow cathode discharge, we use a simple method to separate the sheath region characterized by drastic changes of plasma parameters and the bulk plasma region characterized by smooth changes of plasma parameters. A zero-dimensional chemical kinetic model is used to analyze the dissociation mechanism of CO_2 in the bulk plasma region of a micro-hollow cathode discharge and is validated by comparisons with previous modeling and experimental results. The analysis of the chemical kinetic processes has shown that the electron impact dissociation and heavy species impact dissociation are dominant in different stages of the micro-hollow cathode discharge process for a given applied voltage. The analysis of energy consumption distributions under different applied voltages reveals that the main reason of the conversion improvement with the increase of the applied voltage is that more input energy is distributed to the heavy species impact dissociation.

PACS: 82.33.Xj, 52.80.Mg, 52.27.−h DOI: 10.1088/0256-307X/33/10/108201

During the past decades, there has been a growing concern of climate change owing to the growing concentration of CO_2 in the atmosphere as well as an increasing interest in the mitigation of this issue through the dissociation and conversion CO_2 into added value products.[1] Thermal methods for CO_2 conversion have been successful, but they are not feasible from an energy efficiency standpoint.[2] Therefore, applications of nonequilibrium plasma technologies to reduce large energy cost of CO_2 dissociation have attracted much attention.[3,4] In some situations, it has been found that nonequilibrium plasmas are capable of achieving highly energy-efficient dissociation, which is a key component to scale up the technology for industrial-size applications. Recently, an experimental study on dissociating CO_2 by using the plasma reactor of micro-hollow cathode discharge (MHCD) has shown that the maximum energy conversion efficiency of 14% and CO yield of 10.5% are achieved, which demonstrate that the MHCD plasma reactor can be a promising technology.[4] The effects of some important operational parameters, such as the applied voltage, the gas flow rate on CO_2 dissociation performance of the MHCD reactor, have also been reported. However, the dissociation mechanism of CO_2 in the MHCD reactor, which is due to the complex multi-step nature of the dissociation process, involving many vibrational levels, is not well understood.

To understand and optimize the plasma-assistant CO_2 decomposition process, thorough insight into the plasma chemistry is needed. However, in consideration of the complex chemical kinetics of CO_2 dissociation including thousands of processes,[5−7] it is too difficult to simulate MHCD based on two- or three-dimensional numerical models before a simple but rational chemical kinetic model has been obtained. Therefore, we focus on the analysis of the dissociation processes within MHCD based on a zero-dimensional model, in which the time evolution of the densities of the various plasma species caused by plasma chemical processes are calculated in a given simulation volume, where all plasma parameters including pressure, temperature, reduced electric field are assumed to be spatially homogeneous, and transport phenomena can be ignored.[8] Mathematically, the zero-dimensional model is expressed as a number of coupled ordinary differential equations of these various plasma species,

$$\frac{dn_i}{dt} = \sum_j [(a_{ij}^{\mathrm{R}} - a_{ij}^{\mathrm{L}})k_j \prod_l n_l^{\mathrm{L}}], \tag{1}$$

where n_i is the density of species i, a_{ij}^{R} and a_{ij}^{L} are the right-hand side and left-hand side stoichiometric coefficients of species i in the reaction j, respectively, k_j is the reaction rate constant, and n_l^{L} is the density of the lth reactant of reactions j. The Boltzmann equation is coupled with Eq. (1) to solve the electron energy distribution function (EEDF). The reaction rates for electron impact reactions can be calculated by the EEDF and the corresponding collision cross sections.[6] The rate coefficients for the other gas phase reactions adopted from literature are expressed as functions of electron temperature and gas temperature. An open-source code ZDPlasKin[9] is used to solve Eq. (1), and the module BOLSIG+[10] is called automatically to solve the Boltzmann equation whenever the plasma parameters change significantly.

The species included in the model are presented in Table 1. Eight neutral species (i.e., ground state molecules and radicals which are related to CO_2 and

*Supported by the National Natural Science Foundation of China under Grant Nos 11575019 and 11275021.

**Corresponding author. Email: whx@buaa.edu.cn

© 2016 Chinese Physical Society and IOP Publishing Ltd

O_2) are taken into account, as well as 11 different positive ions and 6 different negative ions. Several excited levels of CO_2, CO, O_2 are also included. For CO_2, previous studies have shown that the vibrational levels, especially highly excited asymmetric mode levels of CO_2, play important roles in the dissociation processes.[6,7] Therefore, asymmetric mode vibrational levels are considered up to 5.47 eV, which is close to the dissociation energy of 5.5 eV, denoted as CO_2v_1, CO_2v_2,..., CO_2v_{21} in Table 1. Only four effective levels of symmetric mode vibrations are considered in this model, which are denoted by letters, i.e. CO_2v_a, CO_2v_b, CO_2v_c, CO_2v_d. The two lowest electronic excitation levels of CO_2 are included in the study, denoted as CO_2e_1 and CO_2e_2. For CO, the first 10 vibrational levels up to 2.51 eV are included, denoted as COv_1, COv_2,..., COv_{10} in Table 1. The electronic excitations of CO have been grouped in four different levels, which are denoted as COe_1, COe_2, COe_3 and COe_4, respectively. For O_2, four vibrational states, which are denoted as O_2v_1, O_2v_2, O_2v_3 and O_2v_4,, and two electronic excitation states are included.

Table 1. All species in the model.

Neutrals and radicals	CO_2, CO, C_2O, C, C_2, O_2, O_3, O
Positive ions	CO_2^+, CO_4^+, CO^+, $C_2O_2^+$, $C_2O_3^+$, $C_2O_4^+$, C^+, C_2^+, O_2^+, O_4^+, O^+
Negative ions	CO_3^-, CO_4^-, O^-, O_2^-, O_3^-, O_4^-
Excited states	CO_2v_1, CO_2v_2,... CO_2v_{21}, CO_2e_1, CO_2e_2, CO_2v_a, CO_2v_b, CO_2v_c, CO_2v_d, COv_1, COv_2,... COv_{10}, COe_1, COe_2, COe_3, COe_4, O_2v_1, O_2v_2, O_2v_3, O_2v_4, O_2e_1, O_2e_2

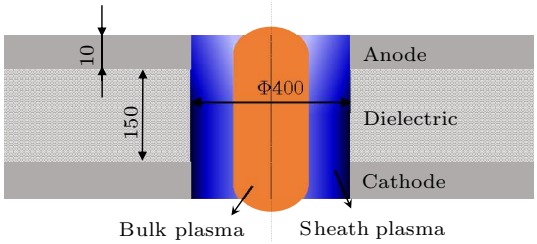

Fig. 1. Schematic profile of MHCD (in units of μm).

Three kinds of reactions are included in this chemical kinetic model, i.e., electron impact reactions, heavy species reactions involving a change of vibrational energy and heavy species chemical reactions. In vibrational energy exchange reactions, the vibrational energy can be lost to translational energy (VT relaxation), exchange among two modes of vibration (VV′ relaxation), or exchange among two molecules in the same mode of vibration (VV relaxation). The whole reaction set in the present model is similar to the chemical kinetic model used in Ref. [6]. The details about the computations of all kinds of reaction rate coefficients can be found in Refs. [5–7].

As mentioned above, MHCD is miniature direct current discharge that can be operated at atmospheric pressure. Previous study has shown that the microdischarge structure is highly inhomogeneous.[11–13] Therefore, the direct application of zero-dimensional kinetic model to analyze dissociation processes of CO_2 would lead to large error. However, if we carefully investigate the features of plasma parameters inside MHCD, it would be found that the MHCD is characterized by a distinct sheath region characterized by drastic changes of plasma parameters and a bulk plasma region characterized by smooth changes of plasma parameters, as shown in Fig. 1. For example, in the MHCD for the case with helium as the working gas, the electron density maintains around 10^{12}–10^{14} cm^{-3} in the bulk plasma region and drops rapidly in the sheath region.[12] Hence, the application of the zero-dimensional model in the bulk region with relatively homogeneous plasma parameter distribution is more reasonable than that in the sheath region.

The small geometric dimensions in MHCD have limited detailed quantitative experimental diagnostic studies of their properties, thus a simple method is introduced to estimate the sheath thickness in the MHCD in this study,[14]

$$s = \left(\frac{9\varepsilon_0\mu_i V_0^2}{8J_0}\right)^{1/3} = \left(\frac{9\varepsilon_0\mu_i V_0^2}{8en_s u_s}\right)^{1/3}, \qquad (2)$$

where s is the sheath thickness, ε_0 is the vacuum permittivity, μ_i is the mobility of ion, V_0 is the voltage between electrodes, e is the electron charge, J_0 is the current density, and n_s and u_s are the ion density and velocity values at the sheath edge, respectively. The input parameters used in this simulation are the same as the operating parameters in Ref. [4]. In Taylan's experiment, the MHCD reactor was operated at an applied dc voltage of 2.5–4.5 kV in a CO_2 flow rate of 100 ml/min. It is noted that the applied voltage is much higher than that in usual situations. This is due to the fact that the breakdown voltage for pure CO_2 is estimated to be 2.1 kV using a Townsend breakdown mechanism based on the atmospheric pressure and the size of the discharge hole used in this experiment. Hence, based on this estimated value and the voltage limit of the power supply, the applied dc voltage varies from 2.5 to 4.5 kV. In the situation of the applied voltage 4.5 kV, the self-pulsing regime is observed through voltage and current measurements. The currents of 1–12 mA and the voltages of 200–1800 V between electrodes are taken from the voltage and current characteristics presented in Fig. 3 of Ref. [4]. An average value of the voltages of 1000 V between electrodes and the electron density on the order of 10^{12}–$10^{13}$$cm^{-3}$ at

the sheath edge are adopted in the estimation. The ion mobility is taken to be $1.133\,\mathrm{cm^2V^{-1}s^{-1}}$, which is measured from Ar-CO_2 mixtures.[15] The thickness of sheath predicted by Eq. (2) is about 70–150 μm. In the previous studies,[11–13] the micro-discharge has been found to have a bulk plasma region and a cathode sheath region with sizes that are comparable. For example, the thickness of sheath is one quarter of the radius of hole when using helium as the working gas.[12] For the case of argon, it has been found that the sheath thickness achieves half the radius or even exceeds the radius of hole depending on the different operating parameters.[13] Hence, the estimated sheath thickness by this method is reasonable. Then, the sheath thickness of 100 μm, i.e., the bulk plasma diameter of 200 μm, is adopted in the following calculation of the zero-dimensional chemical kinetic model.

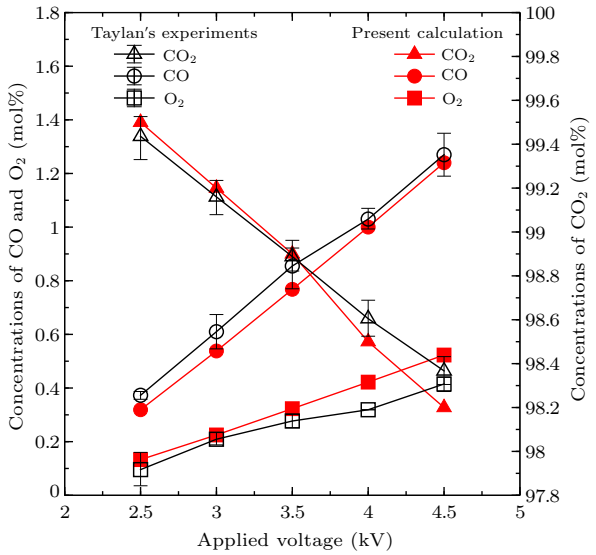

Fig. 2. Comparison with Taylan's experimental results.

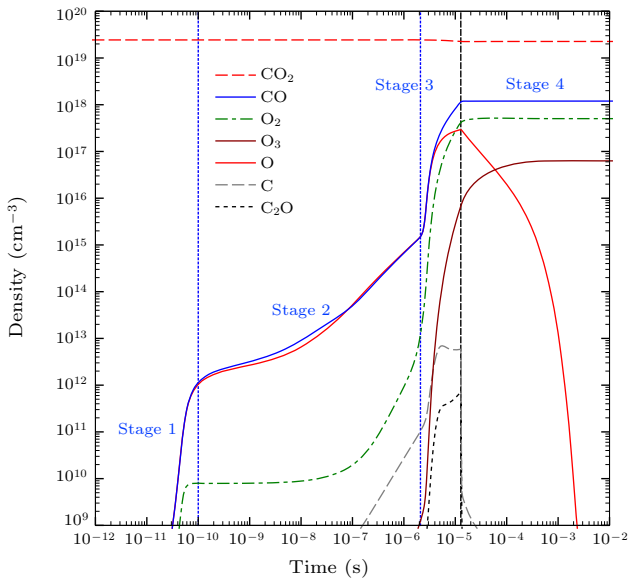

Fig. 3. Densities of important neutral species as a function of time.

The validation of the code and chemical kinetic model is performed through comparison with the experimental results from Ref. [4]. The comparisons between the predicted and measured concentrations of CO, O_2 and CO_2 in the reactor as a function of the applied voltage at a flow rate of 100 ml/min are plotted in Fig. 2. Generally, the predicted conversions by our model agree well with the experimental results. The agreement with the experimental results under these conditions is a verification of the reliability of the chemical kinetic model and the reasonability of estimation method for the sheath size inside the MHCD.

To better understand the dissociation processes in the MHCD, the chemical kinetic processes in bulk plasma are analyzed under the condition of the applied voltage 4.5 kV.

Based on the flow rate of 100 ml/min and the size of the MHCD device with 400 μm in diameter and 150 μm in length, one can obtain the reaction residence time of 12.8 μs, as presented in Ref. [4]. Figure 3 illustrates the temporal evolution of neutral species during the discharge process. Three vertical dashed lines are added in this figure to indicate four stages of dissociation processes. At the initial stage of the discharge, although the reduced electric field (E/N) is high, the dissociation process is not apparent before 10^{-11} s, due to the fact that electron density is quite low in this stage. With the increase of the electron density which is due to the ionization of CO_2, the dissociation will have the first obvious increasing rate, at 10^{-10} s in stage 1. The second stage is the transitional process, in which large numbers of vibrational level species are produced. The densities of dissociation species increase relative slowly in this stage. In the third stage, the heavy species impact dissociations become dominant with the increase of high vibrational level densities, which lead to the significant increase of dissociation species. Finally, the important species of CO and O_2 achieve equilibrium in the fourth stage, which corresponds to the situation that the plasma leaves the discharge domain.

Time-dependent analyses of vibrational temperatures and EEDFs are, respectively, shown in Figs. 4(a) and 4(b). The vibrational temperatures of the asymmetric mode of CO_2 and CO increase from 10^{-9} s, while the vibrational temperature of symmetric mode of CO_2 increases after 10^{-6} s, as shown in Fig. 4(a). The vibrational levels of the asymmetric mode of CO_2 have a great contribution to the dissociation processes when the temperatures reach the peak value of about 2600 K at 2×10^{-6} s, corresponding to the third stage in Fig. 3. At the end of discharge stage, the vibrational temperatures of CO and the symmetric mode of CO_2 exceed the asymmetric mode of CO_2, due to the frequent energy transfer between CO_2 and CO through vibrational-vibrational energy relaxations. After the plasma leaving the discharge domain, all the vibrational temperatures will decrease to the environmental

temperature 300 K. The four lines in Fig. 4(b) represent the EEDFs at the initial time of four stages. It can be seen that the EEDF at the initial time of the first stage has much higher energy tail than that of the third stage, which leads to the fact that the electron impact ionization has a higher reaction rate than other reactions except for the reaction of second electronically excited process in the first stage, as shown in Fig. 5(a). The strong electron impact ionization in the first stage provides enough electrons to maintain the discharge in the MHCD. In the second stage, a large amount of the CO_2 molecules are excited to the vibrational levels, which leads to the significant increase of dissociation through the heavy species impact reactions in the third stage.

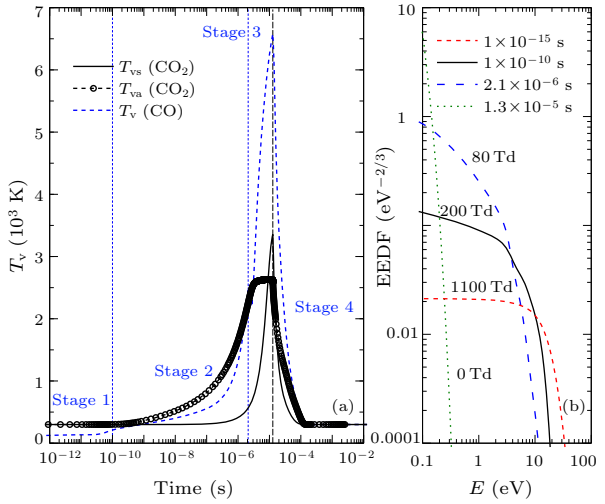

Fig. 4. (a) Time dependence of vibrational temperatures of CO_2, symmetric mode T_{vs} (CO_2), asymmetric mode T_{va} (CO_2), and vibrational temperature of CO, T_v (CO). (b) EEDFs in different discharge stages.

Figure 5(b) plots the temporal evolution of three kinds of dissociation rates. It can be seen that the electron impact dissociation has a higher rate than other dissociations during the first stage. With the development of the discharge in the MHCD, the concentrations of vibrational level species increase, and the vibrational temperatures also increase, as described in Fig. 4(a). In the third stage, the asymmetric vibrational temperature reaches the highest values, the rates of heavy neutral species impact dissociation (D_M, M+CO_2 (ground, vibration, excitation)→CO+O+M) and the oxygen atom impact dissociation (D_O, O+CO_2 (g, v, e)→CO+O_2) rise rapidly and become the dominant processes.

The analysis of energy distribution during the discharge process is useful to understand the dissociation mechanism of CO_2 in the MHCD. Figure 6(a) presents the temporal evolution of energy consumption for different kinetic processes. The electronically excited reactions cost most of the energy input, corresponding to their greater rates than other reactions in the first stage in Fig. 5(a). The energy consumed by electronically excited reactions can produce numerous species of electronically excited states, which easily return to the ground state. During the de-excitation process of electronically excited states, the energy is transferred to translational energy used to raise the heavy species temperature and is not very useful for the dissociation. With the development of the discharge process, the energy absorbed by vibrational levels achieves 60% of the total energy input, and some of the high energy vibrational levels can be further dissociated due to the lower threshold energy for dissociation. However, it has been shown in Fig. 6(a) that only less than half the vibrational energy will be used for CO_2 dissociation through the heavy neutral species impact dissociation (D_M) and the oxygen atom impact dissociation (D_O). Most of the vibration energy of CO_2 is lost through the channels of vibrational-translational energy exchange (VT), asymmetric vibrational-asymmetric vibrational energy exchange (VV), asymmetric vibrational-symmetric vibrational energy exchange (VV′), and vibrational energy of CO_2-vibrational energy of CO exchange (VV_{CO}). During these processes, VV′ and VV_{CO} relaxations consume the partial vibrational energy to raise the symmetric vibrational temperature of CO_2 and the vibrational temperature of CO, as plotted in Fig. 4(a).

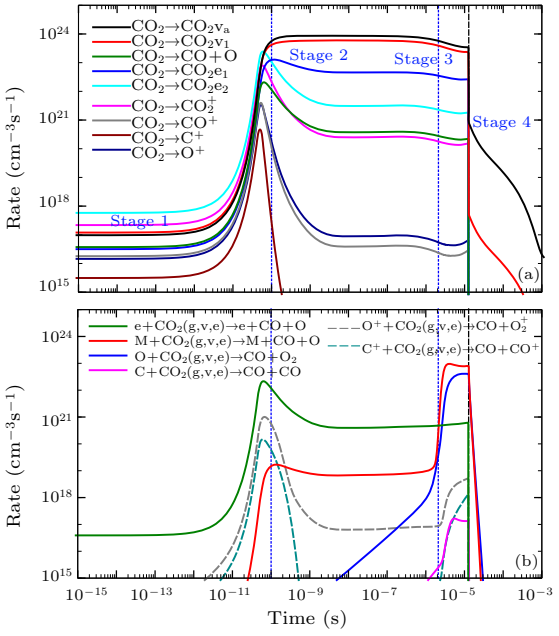

Fig. 5. Rates of (a) electron impact reactions and (b) dissociation reactions as a function of time.

The effects of applied voltages on the energy fraction consumed by different kinetic processes during the MHCD are also investigated in this study. As shown in Fig. 6(b), the change of the applied voltage has slight influence on the energy on consumption of the electronically excited reactions, while the energy used by heavy neutral species impacts dissociation (D_M) and the oxygen atom impact dissociation (D_O) increases with the applied voltage. This is due

to the fact that with the increase of the applied voltage, the electron density in the bulk region increases, which leads to the increase of high vibrational excited levels of CO_2. The increase of high excited levels of CO_2 will promote the dissociations through the heavy neutral species impact dissociation (D_M) and the oxygen atom impact dissociation (D_O). Since more vibrational excited levels of CO_2 are dissociated in the cases with high applied voltages, the energy fraction lost through the channels of VT, VV, VV′, and VV_{CO} will be decreased.

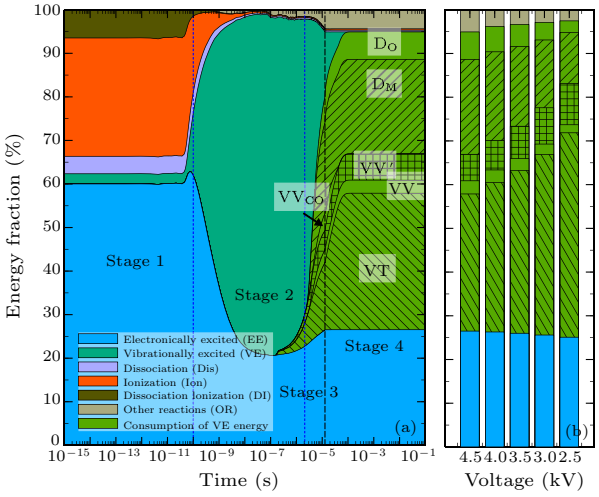

Fig. 6. (a) Temporal evolution of energy consumption for different processes. (b) Energy distribution among the different processes for different applied voltages.

In summary, a zero-dimensional model of CO_2 dissociation has been used in the bulk plasma region of the MHCD to investigate the dissociation mechanism during the discharge process. A simple reasonable method of estimating the sheath size is introduced based on the structure features of the MHCD. The validation of the method and the model has been performed by the comparisons with the modeling and experimental results. The analysis of the temporal evolution of chemical kinetic processes shows that electron impact dissociation and heavy species impact dissociation are dominant in different stages of the MHCD. The energy distribution among the different kinetic processes during the discharge process is also analyzed for the typical situation. It is found that most of the vibration energy of CO_2 is lost through the energy transfer channels between the heavy species. Only a small part of vibrational energy is used for CO_2 dissociation through the heavy neutral species impact dissociation and the oxygen atom impact dissociation.

References

[1] Lebouvier A, Iwarere S A, d'Argenlieu P et al 2013 *Energy Fuels* **27** 2712
[2] Huczko A and Szymański A 1984 *Plasma Chem. Plasma Process.* **4** 59
[3] Horváth G, Skalný J D and Mason N J 2008 *J. Phys.* D **41** 225207
[4] Taylan O and Berberoglu H 2015 *Plasma Sources Sci. Technol.* **24** 15006
[5] Aerts R, Martens T and Bogaerts A 2012 *J. Phys. Chem.* C **116** 23257
[6] Kozák T and Bogaerts A 2014 *Plasma Sources Sci. Technol.* **23** 45004
[7] Kozák T and Bogaerts A 2015 *Plasma Sources Sci. Technol.* **24** 15024
[8] Sun S R and Wang H X 2014 *Chin. Phys. Lett.* **31** 095205
[9] Pancheshnyi S, Eismann B, Hagelaar G J M and Pitchford L C *Computer Code ZDPlasKin* http://www.zdplaskin.laplace.univ-tlse.fr
[10] Hagelaar G J M and Pitchford L C 2005 *Plasma Sources Sci. Technol.* **14** 722
[11] Kushner M J 2005 *J. Phys.* D **38** 1633
[12] Kothnur P S and Raja L L 2005 *J. Appl. Phys.* **97** 43305
[13] Deconinck T and Raja L L 2009 *Plasma Processes Polym.* **6** 335
[14] Lieberman M A and Lichtenberg A J 2005 *Principles of Plasma Discharges and Materials Processing* (New Jersey: John Wiley & Sons) p 184
[15] Encarnação P M C C, Cortez A F V, Pinto M G A et al 2015 *J. Instrum.* **10** P1010